BLE-Based AoA Estimation Using a Sliding Window Median Filter to Remove Outliers

Erick Adrian Iglesias Rodriguez, Marcos Eduardo Pivaro Monteiro, Glauber Brante, Guilherme Luiz Moritz, and Richard Demo Souza

***Abstract*— We propose a method to enhance Bluetooth Low Energy (BLE) angle of arrival (AoA) estimation using the multiple signal classification (MUSIC) algorithm as a base estimator. In order to identify and remove outliers that jeopardize the accuracy performance, the proposed algorithm employs a sliding window median filter, which is compared to an adjustable threshold. Experiments with a 4×4 uniform rectangular array receiving signals from three BLE tags show that the proposed method reduces the root mean squared error by 54.9% compared to traditional MUSIC. Furthermore, the probability of achieving measurement errors below 5° increases from 77% to 83% with the proposed scheme, improving the AoA accuracy.**

***Keywords*— Angle of Arrival, Moving Median Filter, MUSIC algorithm.**

I. Introduction

The relevance of the Internet of Things (IoT) continues to grow, leading to widespread recognition of its potential in both industry and among technology consumers, with the number of IoT devices and their associated market value continuing to rise significantly. Among different applications, several require higher accuracy in indoor positioning. For instance, tracking and localization for the industry, as well as fall detection systems for elderly people, depend on enhanced accuracy and good indoor positioning mechanisms [1]. Indoor positioning can be achieved by means of fingerprinting, multilateration, and triangulation, among others [2]. Fingerprinting techniques require a device-based calibration phase to map the received signal strength indicator (RSSI) in a given environment. Multilateration methods use the estimated distance of the device, while triangulation usually employs the angle of arrival (AoA) to estimate positioning. As a result, indoor positioning accuracy depends on specific metrics such as RSSI, AoA, channel state information (CSI), time of flight (ToF), or channel impulse response (CIR).

Nevertheless, CIR and CSI are not readily available on commercial devices. RSSI, although available on most devices, is susceptible to multipath effects and interference. ToF requires precise synchronization between the transmitter and receiver, with localization errors increasing in non-line-of-sight conditions. Meanwhile, AoA can provide accurate estimations if the far-field and good line-of-sight conditions between the transmitter and receiver are satisfied. Thus, even though its accuracy decreases with the distance, AoA shows great potential for providing higher accuracy and faster estimations in indoor positioning, while it is widely employed in indoor localization and positioning systems within the IoT [3].

Localization technologies based on WiFi, ultra-wideband, and Bluetooth commonly employ the AoA method. The Bluetooth Low Energy (BLE) 5.1 specification introduced the constant tone extension (CTE), which is appended to the ordinary BLE packet in order to allow for AoA estimation [4]. As a result, an increasing use of BLE technology is observed in the recent literature [5]–[9]. For instance, the work in [5] builds a system topology and algorithms for BLE-based indoor localization. Experiments were conducted in an anechoic chamber and further expanded to both indoor and outdoor areas. The main goal of the paper was to experimentally obtain the localization accuracy, which achieved a mean absolute error of 3.6 m. Furthermore, the work in [6] presents an AoA estimation algorithm that employs a maximum likelihood (ML)-weighted iterative approach to estimate both the carrier frequency offset (CFO) and AoA jointly using a circular antenna array. Despite the complexity of the ML approach, the accuracy in AoA with respect to the multiple signal classification (MUSIC) algorithm [10] is increased by 10%.

Similarly, the authors in [7] proposed a method that combines nonlinear recursive least squares and Kalman filtering in order to deal with the multipath and noise effects in the baseband in-phase (I) and quadrature (Q) samples associated with the CTE. Results show that the average AoA estimation error can be decreased by 3.9° compared to MUSIC. The multipath effect of the wireless channel has also been investigated in [8], which combines nonlinear least squares, zero-forcing equalization, and fast Fourier transform to deal with noise and fading. Based on simulation results employing a Rayleigh fading channel, the proposed approach illustrates accuracy improvements with respect to the MUSIC algorithm. In addition, the authors in [9] propose a method employing signal fitting combined with the propagator direct data acquisition (PDDA) angle estimation algorithm. This approach circumvents the need to compute phase differences between antennas, thus reducing computational complexity. However, despite being less computationally intensive, the PDDA method does not offer improved accuracy compared to MUSIC.

Traditional AoA approaches are generally categorized into three main types: conventional beamforming algorithms, subspace decomposition methods, and parametric techniques [11], [12]. Conventional beamforming includes the

E. A. I. Rodriguez, M. E. P. Monteiro, G. Brante and G. L. Moritz are with the Federal University of Technology, Curitiba-PR, e-mails: erick.2023@alunos.utfpr.edu.br, {marcose, gbrante, moritz}@utfpr.edu.br. Richard Demo Souza is with the Federal University of Santa Catarina, Florianópolis-SC, e-mail: richard.demo@ufsc.br. This work was partially supported by CAPES, Finance Code 001, CNPq (305021/2021-4, 307226/2021-2), Agência Nacional de Energia Elétrica (ANEEL) and Celesc Distribuição S.A. under the research and development program (project PD05697-1323/2023).

Bartlett method [13], while subspace decomposition methods feature algorithms such as MUSIC [10], estimation of signal parameters via rotational invariance techniques (ESPRIT) [14], and the Capon method [11]. Finally, parametric methods encompass techniques such as space-alternating generalized expectation-maximization (SAGE) and ML estimation [3]. In this work, subspace decomposition estimation using MUSIC has been chosen over other methods because it provides statistically consistent estimates in contrast to the beamforming techniques, while also being computationally attractive compared to parametric methods [12]. Furthermore, the MUSIC became a benchmarking alternative to most existing methods, being less complex than parametric methods [11], [12] and more accurate than ESPRIT [15].

In this paper, we aim to classify the quality of the AoA measurements, discarding bad AoA estimates. Such feature is critical to enabling practical, real-world applications, while the literature is vague in addressing this issue. The proposed method is designed to remove outliers as the measurements are processed, so we propose an algorithm based on a sliding window median filter, which is further compared to an adjustable threshold. Thus, every new AoA estimate obtained by the MUSIC algorithm is compared to the median of the N previous valid estimates. If the measurement quality does not fit the designed threshold, it is considered an outlier and is discarded. In order to validate our method, we have conducted experiments with a 4×4 uniform rectangular array (URA) receiving signals from three BLE tags. Results show that the proposed method reduces the root mean squared error (RMSE) by 54.9% compared to traditional MUSIC, while the probability of achieving measurement errors below $5°$ increases from 77% to 83% with the proposed scheme.

II. Fundamentals

To perform AoA measurements, the receiver must be equipped with an antenna array, so that the AoA estimates using the received signal provide an elevation angle θ and an azimuth angle ϕ. In the case of a URA, with M_{X} antenna elements in the horizontal direction and M_{Y} antenna elements in the vertical direction, the total number of antenna elements is $M = M_{\mathrm{X}} \times M_{\mathrm{Y}}$. In addition, the distance between the centers of the array elements in the two directions are denoted by d_{X} and d_{Y}, respectively.

At the URA, the received signal at time t is denoted by $\boldsymbol{x}(t) = [x_1(t), x_2(t), \ldots, x_M(t)]^T$, with $(\cdot)^T$ denoting the transpose operation. Then, $\boldsymbol{x}(t)$ can be written as [10], [11]

$$\boldsymbol{x}(t) = \mathbf{A}\boldsymbol{s}(t) + \boldsymbol{n}(t), \tag{1}$$

where $\boldsymbol{s}(t) = [s_1(t), s_2(t), \ldots, s_p(t)]^T$ is an attenuated version of the transmitted signal, p is the number of signal sources captured by the receiver, $\boldsymbol{n}(t) = [n_1(t), n_2(t), \ldots, n_M(t)]^T$ is the zero-mean additive white Gaussian noise, with spatial covariance matrix $\sigma_N^2 \mathbf{I}_M$, where σ_N^2 is the noise variance and $\mathbf{I}_M$ the identity matrix of size M, while $\mathbf{A} \in \mathbb{C}^{M \times p}$ is the steering matrix, given by

$$\mathbf{A} = [\boldsymbol{a}(\theta_1, \phi_1), \boldsymbol{a}(\theta_2, \phi_2), \ldots, \boldsymbol{a}(\theta_p, \phi_p)], \tag{2}$$

in which $\boldsymbol{a}(\theta_i, \phi_i)$, $i \in [1, p]$, denotes the steering vector for the i-th signal source [10], [11]. In the case of URA, it can be expressed as [11] $\boldsymbol{a}(\theta_i, \phi_i) = \boldsymbol{a}_{\mathrm{Y},i} \otimes \boldsymbol{a}_{\mathrm{X},i}$, where $\otimes$ denotes the Kronecker product, while $\boldsymbol{a}_{\mathrm{X},i} = \left[1, e^{j\psi_{\mathrm{X},i}}, \ldots, e^{j(M_{\mathrm{X}}-1)\psi_{\mathrm{X},i}}\right]^T$, $\boldsymbol{a}_{\mathrm{Y},i} = \left[1, e^{j\psi_{\mathrm{Y},i}}, \ldots, e^{j(M_{\mathrm{Y}}-1)\psi_{\mathrm{Y},i}}\right]^T$, with $\psi_{\mathrm{X},i} = 2\pi d_{\mathrm{X}} \lambda^{-1} \cos\theta_i \sin\phi_i$, $\psi_{\mathrm{Y},i} = 2\pi d_{\mathrm{Y}} \lambda^{-1} \sin\theta_i \sin\phi_i$, and λ being the wavelength.

A. MUSIC Subspace Decomposition

The MUSIC algorithm estimates the AoA of the signal sources from $\boldsymbol{x}(t)$ by performing eigen-decomposition of the covariance matrix $\mathbf{R}_{xx} = \mathbb{E}[\boldsymbol{x}\boldsymbol{x}^H]$ of the received signal [10], [11], where $(\cdot)^H$ denotes the Hermitian transpose operation and $\mathbb{E}[\cdot]$ is the mathematical expectation. By assuming that all underlying random noise processes are ergodic, the statistical expectation can be replaced by a time average, so that for N snapshots we have that [11]

$$\mathbf{R}_{xx} = \frac{1}{N} \sum_{n=1}^{N} \boldsymbol{x}(t_n)\boldsymbol{x}^H(t_n), \tag{3}$$

where t_n is the time instant of the n-th snapshot.

In addition, in a multipath environment, the signals arriving at the array are often highly correlated, so the forward-backward (FB) averaging is usually employed to obtain more reliable estimates [11], defined as

$$\mathbf{R}_{xx}^{\mathrm{FB}} = \frac{1}{2}\left(\mathbf{R}_{xx} + \mathbf{J}_M \mathbf{R}_{xx}^* \mathbf{J}_M\right), \tag{4}$$

where $(\cdot)^*$ denotes the conjugate operation and $\mathbf{J}_M$ is the $M \times M$ anti-identity matrix, with ones on its anti-diagonal and zeros elsewhere. The new FB covariance matrix $\mathbf{R}_{xx}^{\mathrm{FB}}$ has rank p, assuming that $p < M$ sources are captured by the receiver, and it enables the separation of coherent or highly correlated signals.

Then, the eigenvalue decomposition (EVD) of (4) yields

$$\mathbf{R}_{xx}^{\mathrm{FB}} = \mathbf{U}\mathbf{\Lambda}\mathbf{U}^H = \mathbf{U}_S\mathbf{\Lambda}_S\mathbf{U}_S^H + \mathbf{U}_N\mathbf{\Lambda}_N\mathbf{U}_N^H, \tag{5}$$

where $\mathbf{\Lambda}$ is an $M \times M$ diagonal matrix containing the eigenvalues of $\mathbf{R}_{xx}^{\mathrm{FB}}$, while $\mathbf{U}$ is an $M \times M$ matrix whose columns are the eigenvectors of $\mathbf{R}_{xx}^{\mathrm{FB}}$. Moreover, $\mathbf{U}$ can be further decomposed into the signal subspace $\mathbf{U}_S \in \mathbb{C}^{M \times p}$ and the noise subspace $\mathbf{U}_N \in \mathbb{C}^{M \times (M-p)}$.

Finally, the MUSIC algorithm exploits the fact that the noise subspace is orthogonal to the signal subspace. The MUSIC spectrum is given by [10], [11]

$$P(\theta_i, \phi_i) = \frac{1}{|\boldsymbol{a}^H(\theta_i, \phi_i)\mathrm{U}_N\mathrm{U}_N^H\boldsymbol{a}(\theta_i, \phi_i)|}, \tag{6}$$

whose denominator represents a measure of the degree of orthogonality of the steering vector for direction (θ_i, ϕ_i) with respect to the noise subspace. A higher degree of orthogonality with respect to the noise yields a denominator closer to zero, generating a peak in the MUSIC spectrum. Then, the AoAs of the signal sources can be estimated by finding the angles corresponding to peaks in $P(\theta_i, \phi_i)$.

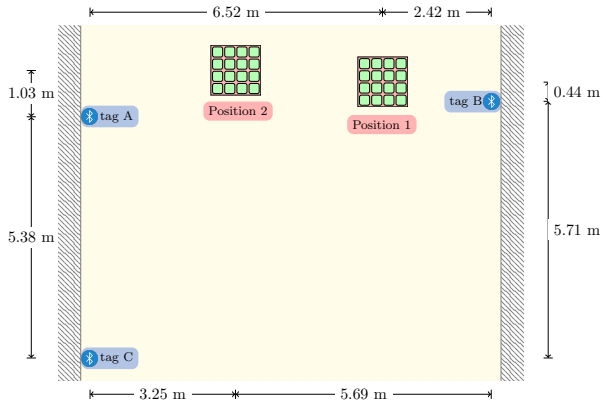

Fig. 1. Two different positions for the URA and the tags A, B, and C.

TABLE I
TRUE AZIMUTH AND DISTANCE MEASUREMENTS FROM THE URA TO THE TAGS A, B, AND C.

Experiment Label	Tag	URA Position	True Azimuth	Distance
P1A	A	1	$-85.1°$	6.54 m
P1B	B	1	$79.6°$	2.46 m
P1C	C	1	$-46.4°$	9.00 m
P2A	A	2	$-72.4°$	3.41 m
P2B	B	2	$83.8°$	5.72 m
P2C	C	2	$-26.4°$	7.32 m

III. Proposed Scheme

In this section, we describe the experimental setup used to evaluate the MUSIC algorithm's performance, while we also introduce the proposed method to classify the quality of the AoA estimates, discarding outliers.

A. Experimental Setup

The experiment was conducted using three BLE Thunderboard EFR32BG22 transmitters [16], which we denote as tags, configured with 160 μs CTE packets transmitted with 0 dBm. Also, we have employed a 4×4 URA antenna ($M = 16$) using the EFR32BG22 direction finding radio board (BRD4185A) from Silicon Labs [17], whose antenna elements are spaced by $d_{\mathrm{X}} = d_{\mathrm{Y}} = 0.04$ m. In addition, the experiment was carried out in a room, where the URA was placed in two different positions while the three tags were fixed on the walls. Fig. 1 provides a diagram illustrating the two array positions and the locations of the three tags in the room.

In our analysis, we restrict the scenario to a 2D localization, so that the URA provides IQ samples, which are fed to the MUSIC algorithm to extract the azimuth angle, while the elevation is assumed to be known. Table I outlines six selected cases for the experiments, which are denoted by P1A (URA at Position 1 receiving a transmission from Tag A), P1B (URA at Position 1 receiving from Tag B), P1C (URA at Position 1 receiving from Tag C), P2A (URA at Position 2 receiving from Tag A), and so on. The distance from the tag to the URA and the azimuth angle in this table were measured using a Fluke 414D laser telemeter, with 2 mm precision [18].

TABLE II
RMSE OF THE MUSIC ALGORITHM FOR THE SIX CASES OF TABLE I.

Experiment Label	Average Azimuth	RMSE
P1A	$-50.96°$	$66.23°$
P1B	$77.96°$	$5.28°$
P1C	$-48.93°$	$7.54°$
P2A	$-70.38°$	$6.00°$
P2B	$65.28°$	$38.11°$
P2C	$-28.47°$	$7.07°$

Furthermore, we use the root mean squared error (RMSE) with respect to the true azimuth value of Table I as the evaluation metric, which is defined as

$$\mathrm{RMSE} = \sqrt{\frac{1}{N}\sum_{n=1}^{N}\left(\phi_{\mathrm{estimated}}(t_n) - \phi_{\mathrm{measured}}\right)^2}, \qquad (7)$$

where $\phi_{\mathrm{estimated}}(t_n)$ comes from the MUSIC algorithm at time t_n, while ϕ_{measured} is the measured azimuth angle.

B. Azimuth Estimations Using MUSIC

As an initial analysis, we have run the MUSIC algorithm to estimate the AoA for each of the six cases depicted in Table I. A total of 10.000 CTEs have been collected, and Table II summarizes the results in terms of the average estimated azimuth angle and the RMSE relative to the true azimuth. As we observe, MUSIC provides good estimates for some positions, *e.g.*, P1B, P1C, P2A, and P2C, with RMSE values ranging from $5.28°$ to $7.54°$. However, positions P1A and P2B exhibit very poor performance, with RMSE values up to $66.23°$. Such variation in performance can be due to several factors, such as reflections in windows or other objects of the room, or other interference sources operating at the same frequency as the BLE.

In order to better understand the obtained high RMSE values, Fig. 2 plots histograms for the azimuth estimations at positions P1A, P2B, and P1B. As we observe, the vast majority of the estimations converge to near the true azimuth value. For instance, by taking the mode of the measurements for P1A, *i.e.*, the value with higher occurrence in the histogram, we obtain $-89°$, which is close to the true azimuth of $-85.1°$ from Table I. Similarly, the mode for the measurements at P2B is $81°$, which is close to the true azimuth of $83.8°$. However, what differs from the histograms for P1A and P2B (with high RMSE) from the histogram for P1B is the presence of outliers in a very wide range of azimuth angles. Therefore, identifying outliers is crucial to improve the MUSIC performance.

C. Proposed Scheme to Filter Outliers

Aiming to remove outliers in an online fashion, we propose an algorithm based on a sliding window median filter of N samples, which is further compared to an adjustable threshold T. Thus, every new azimuth estimate obtained by the MUSIC algorithm is compared to the median of the N previous valid estimates. If the absolute value of the difference between the new azimuth estimate and the median is smaller than a

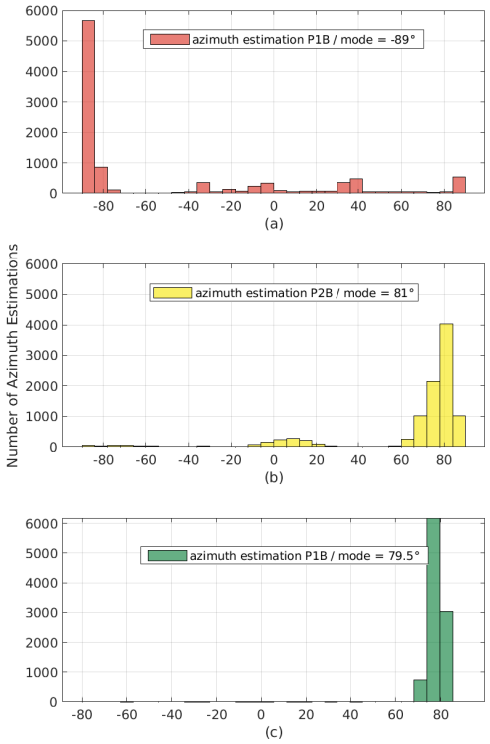

Fig. 2. Histograms of azimuth angle estimations using the MUSIC algorithm for experiments P1A (a), P2B (b), and P1B (c).

Algorithm 1 Proposed Method to Filter AoA Outliers

Require: T, N
1: **for** $\texttt{CTEcount} = 1, \ldots, \texttt{numCTE}$ **do**
2: Compute the new AoA azimuth estimate $\phi(\texttt{CTEcount})$ using the MUSIC algorithm
3: Calculate the median of the N previous azimuth estimations: $\texttt{estimate} = \texttt{median}(\phi(\texttt{CTEcount}-1), \ldots, \phi(\texttt{CTEcount}-N))$
4: Calculate $\texttt{deviation} = |\texttt{estimate} - \phi(\texttt{CTEcount})|$
5: **if** $\texttt{deviation} > T$ **then**
6: Discard $\phi(\texttt{CTEcount})$ estimate
7: $\texttt{numCTE} = \texttt{numCTE} - 1$
8: **end if**
9: **end for**

predefined threshold, the new estimate is considered as *valid*; otherwise, it is considered an *outlier* and it is discarded.

Algorithm 1 details the proposed method to filter the AoA estimates. By denoting $\texttt{CTEcount}$ as the index of the received CTE, we first compute the new azimuth estimate $\phi(\texttt{CTEcount})$ using the MUSIC algorithm (line 2). To determine if $\phi(\texttt{CTEcount})$ is a *valid* measurement or an *outlier* we calculate the median of the N previous azimuth estimations, denoted by the indexes $(\texttt{CTEcount}-1)$ and $(\texttt{CTEcount}-10)$ in line 3 of the algorithm. Then, based on the median, we calculate the absolute value of the difference between variables $\texttt{estimate}$ and $\phi(\texttt{CTEcount})$. If the difference is larger than an established $\texttt{threshold}$ variable, used as the input of the algorithm, then $\phi(\texttt{CTEcount})$ is discarded (line 6), and the total number of $\texttt{numCTE}$ is decremented by one (line 7).

IV. Results

In this section, we evaluate the proposed method compared to the traditional MUSIC algorithm. A total of 10.000 CTEs have been collected by our experimental setup. First, Table III employs the proposed method with different N and T, showing the percentage of discarded samples, which are classified as outliers. The results represent an average across all six cases in Table I. For better visualization, a color gradient from green to red is used to represent increasing percentages of discarded samples. As we observe, the threshold plays a crucial role in the percentage of discarded samples, with small T considerably increasing the number of discarded samples. In order to avoid a high percentage of discarded packets, which implies a longer acquisition time, we establish 20% of discarded samples as a limit for reasonable operation.

Next, we select select two cases for further analysis: *i.)* $(T = 10°, N = 3)$, in which a small N is interesting for algorithmic implementation; and *ii.)* $(T = 8°, N = 7)$, which is the combination with the smallest RMSE among the combinations in Table III, respecting the 20% limit for average percentage of discarded samples. Table IV shows the RMSE and the percentage of discarded samples obtained with these combinations, compared to the traditional MUSIC estimation. As observed, the RMSE is significantly reduced with the proposed method, indicating up to a 50.1% improvement in performance compared to the standard MUSIC algorithm when using $(T = 10°, N = 3)$, and up to a 54.9% improvement with $(T = 8°, N = 7)$. In addition, Table IV also shows the percentage of discarded samples with these two configurations, specifically for each of the six experiment positions. As shown, in order to reduce the RMSE of experiments P1A and P2B, the percentage of discarded samples must be considerably increased.

Fig. 3 shows the RMSE as a function of the SNR of the received CTE samples, comparing the standard MUSIC algorithm with the proposed method using the two selected configurations. The RMSE is an average of the six experiments. Results show that samples with lower SNR tend to produce high RMSE in the MUSIC algorithm, while the proposed algorithm is able to provide more reliable estimates regardless of the SNR.

Finally, Fig. 4 shows the cumulative distribution function (CDF) of the RMSE for experiment P2A. The CDF is obtained by calculating the RMSE of each individual sample with respect to the true azimuth value of the experiment. As we observe, the MUSIC algorithm has 77% probability of obtaining RMSE values smaller than $5°$, while the proposed method increases such probability to 79% with $(T = 10°, N = 3)$, and to 83% with $(T = 8°, N = 7)$, improving the AoA accuracy.

V. Conclusions

In this paper, we proposed a sliding window median filter-based method to improve the AoA estimation using BLE 5.1 and the MUSIC algorithm. New AoA estimates are compared to the median of N previous valid estimates, allowing for the identification of outliers outside a threshold T. To validate our method, we conducted experiments with a 4×4 URA and three

TABLE III

PERCENTAGE OF SAMPLES CLASSIFIED AS OUTLIERS WITH THE PROPOSED METHOD, FOR DIFFERENT N AND T.

	$T = 3°$	$T = 4°$	$T = 5°$	$T = 6°$	$T = 7°$	$T = 8°$	$T = 9°$	$T = 10°$	$T = 11°$	$T = 12°$	$T = 13°$
$N = 10$	53.54	42.70	34.91	29.90	25.26	20.85	17.08	14.44	12.97	12.12	11.53
$N = 9$	50.40	39.86	32.54	27.34	22.76	18.75	15.54	13.52	11.98	11.15	10.53
$N = 8$	52.35	42.19	34.70	29.29	24.73	20.25	16.52	13.74	12.22	11.29	10.63
$N = 7$	51.07	40.46	33.79	27.81	23.20	19.20	15.98	13.83	12.27	11.27	10.57
$N = 6$	52.54	43.28	35.74	30.04	25.34	20.88	17.00	14.02	12.48	11.44	10.70
$N = 5$	52.85	43.14	35.79	30.02	25.38	21.42	18.17	15.86	14.06	12.96	12.19
$N = 4$	54.41	46.17	38.24	31.84	26.91	22.96	19.47	16.97	15.17	13.95	13.18
$N = 3$	52.86	45.88	38.44	31.53	26.61	22.47	19.40	16.69	14.69	13.24	12.11
$N = 2$	57.42	48.18	40.49	33.30	28.34	24.00	20.51	17.76	15.69	14.16	13.02

TABLE IV

RMSE AND PERCENTAGE OF DISCARDED SAMPLES OF THE PROPOSED METHOD WITH $(T = 10°, N = 3)$, AND $(T = 8°, N = 7)$, COMPARED TO THE MUSIC ALGORITHM.

Experiment	**RMSE MUSIC**	**RMSE** $T = 10°$ $N = 3$	**RMSE** $T = 8°$ $N = 7$	**% Discard** $T = 10°$ $N = 3$	**% Discard** $T = 8°$ $N = 7$
P1A	66.23°	11.89°	7.32°	44.99%	41.66%
P1B	5.28°	3.12°	3.11°	0.28%	0.43%
P1C	7.54°	5.16°	4.54°	11.26%	17.50%
P2A	6.00°	4.27°	3.96°	5.64%	8.13%
P2B	38.11°	6.60°	5.66°	27.10%	32.94%
P2C	7.07°	4.61°	4.20°	10.85%	14.55%

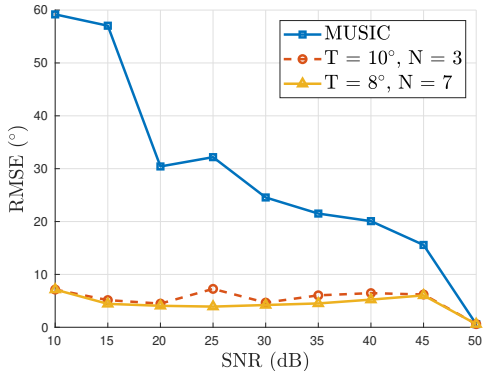

Fig. 3. RMSE vs. the SNR of the received samples comparing the MUSIC algorithm and the proposed method with $(T = 10°, N = 3)$, and $(T = 8°, N = 7)$.

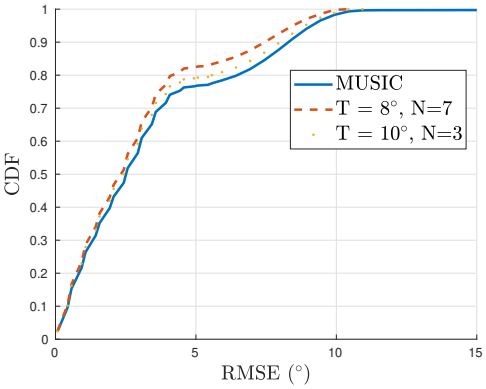

Fig. 4. CDF of the RMSE of the MUSIC algorithm and that of the proposed method with $(T = 10°, N = 3)$, and $(T = 8°, N = 7)$ for P2A.

BLE tags. The results demonstrate the effectiveness of the proposed method in eliminating outliers, achieving an RMSE reduction of over 50%. Furthermore, we have shown that the parameters N and T can be tuned to limit the proportion of discarded AoA samples to no more than 20%. Nevertheless, for certain positions, the percentage of discarded samples must be increased to achieve a lower RMSE. Finally, our results indicate that the proposed method can be used to increase the probability of achieving measurement errors below 5°, raising it from 77% to 83%.

REFERENCES

[1] Y. Hayashi and K. Naito, "Action context estimation method based on AoA of Bluetooth 5.1," in *IEEE International Conference on Consumer Electronics (ICCE)*, 2023, pp. 1–6.

[2] M. Girolami, F. Mavilia, F. Furfari, and P. Barsocchi, "An experimental evaluation based on direction finding specification for indoor localization and proximity detection," *IEEE Journal of Indoor and Seamless Positioning and Navigation*, vol. 2, pp. 36–50, 12 2023.

[3] N. BniLam, R. Janssens, J. Steckel, and M. Weyn, "AoA estimates for LPWAN technologies: Indoor experimental analysis," in *15th European Conference on Antennas and Propagation (EuCAP)*, 2021, pp. 1–5.

[4] S. Bluetooth, "Core specification (amended) version 5.1," 2024.

[5] N. Paulino and L. M. Pessoa, "Self-localization via circular bluetooth 5.1 antenna array receiver," *IEEE Access*, vol. 11, pp. 365–395, 2023.

[6] X. Qiu, B. Wang, J. Wang, and Y. Shen, "AOA-based BLE localization with carrier frequency offset mitigation," in *IEEE International Conference on Communications Workshops (ICC Workshops)*, 2020, pp. 1–5.

[7] S. He, H. Long, and W. Zhang, "Multi-antenna array-based AoA estimation using bluetooth low energy for indoor positioning," in *7th International Conference on Computer and Communications (ICCC)*, 2021, pp. 2160–2164.

[8] Z. Hajiakhondi-Meybodi, M. Salimibeni, A. Mohammadi, and K. N. Plataniotis, "Bluetooth low energy-based angle of arrival estimation in presence of Rayleigh fading," in *IEEE International Conference on Systems, Man, and Cybernetics (SMC)*, 2020, pp. 3395–3400.

[9] H. Ye, B. Yang, Z. Long, and C. Dai, "A method of indoor positioning by signal fitting and PDDA algorithm using BLE AOA device," *IEEE Sensors Journal*, vol. 22, no. 8, pp. 7877–7887, 2022.

[10] R. Schmidt, "Multiple emitter location and signal parameter estimation," *IEEE Transactions on Antennas and Propagation*, vol. 34, no. 3, pp. 276–280, 1986.

[11] H. L. Van Trees, *Optimum array processing: Part IV of detection, estimation, and modulation theory*. John Wiley & Sons, 2002.

[12] H. Krim and M. Viberg, "Two decades of array signal processing research: the parametric approach," *IEEE Signal Processing Magazine*, vol. 13, no. 4, pp. 67–94, 1996.

[13] M. S. Bartlett, "Periodogram analysis and continuous spectra," *Biometrika*, vol. 37, no. 1/2, pp. 1–16, 1950.

[14] R. Roy and T. Kailath, "ESPRIT-estimation of signal parameters via rotational invariance techniques," *IEEE Transactions on Acoustics, Speech, and Signal Processing*, vol. 37, no. 7, pp. 984–995, 1989.

[15] E. Gentilho Jr, P. R. Scalassara, and T. Abrão, "Direction-of-arrival estimation methods: A performance-complexity tradeoff perspective," *Journal of Signal Processing Systems*, vol. 92, no. 2, pp. 239–256, 2020.

[16] Silicon Labs, "UG415: Thunderboard™ EFR32BG22 user's guide," 2021.

[17] ——, "EFR32BG22 direction finding radio board BRD4185A reference manual," 2021.

[18] Fluke, "Fluke414D laser distance telemeter manual," 2024.